doi: 10.82124/CEAS-GNC-2026-012 CEAS-GNC-2026-012

EuroGNC Navigation Guidance Control CEAS Madrid, Spain May 5th-7th uc3m Universidad Carlos III de Madrid AIAA 2026

Fuel-optimal Rendezvous in the CR3BP via MPC and Proximal Operators

Sergio Cuevas del Valle PhD candidate, Universidad Rey Juan Carlos, Móstoles, Spain. sergio.cuevas@urjc.es
GNC Engineer, FOSSA Systems S.L., Madrid, Spain. sergioc@fossa.systems

Hodei Urrutxua Full Professor, Universidad Rey Juan Carlos, Móstoles, Spain. hodei.urrutxua@urjc.es

Pablo Solano-López Assistant Professor, Universidad Rey Juan Carlos., Móstoles, Spain. pablo.solano@urjc.es

ABSTRACT

This work introduces a cost-efficient, closed-form trajectory optimization engine for time-fixed, fuel-optimal rendezvous in the Circular Restricted Three-Body Problem (CR3BP). In particular, Alternating Direction Method of Multipliers –as the numerical solver– and Primer Vector Theory –as the theoretical corpus– are fused together to construct general closed-form, iterative solvers for both constrained and unconstrained $\mathcal{L}_{1,p}$-fuel optimal linear rendezvous problems. To handle uncertainties and model discrepancies, these original solvers are embedded into a Model Predictive Control architecture, leading to an integral suboptimal guidance and control design for the full nonlinear plant dynamics. Moreover, the low footprint and lack of necessary advanced numerical machinery of the resulting design make it a solid candidate for real-time, embedded guidance applications. The integral architecture is applied and extensively validated in several real CR3BP rendezvous mission test cases against state-of-the-art solvers, where its performance is demonstrated.

Keywords: Optimal Rendezvous, CR3BP, Primer Vector Theory, Alternating Direction Method of Multipliers, Model Predictive Control

1 Introduction

During the past years, interest in multi-body missions has bloomed as never before, as demonstrated, for example, by NASA's Artemis program [1]. The design of these new deep-space mission concepts is however constrained by new requirements; this particularly applies for greater autonomy of space probes, and new proximity operations capabilities: deep-space logistics, including the transport of cargo and crew, require of optimized rendezvous, docking and general co-orbital capabilities between spacecraft. In this sense, the design of more capable GNC systems remains as an open challenge for the Space Mechanics community [2].

Multi-body mission analysis and trajectory optimization studies are primarily dominated by the Circular version of the Restricted Three Body Problem (CR3BP), in which the mass of the spacecraft is considered to be negligible with respect to the massive bodies, known as the primaries. Furthermore,

in the CR3BP, the co-orbital state between the primaries is described by a planar circular Keplerian orbit. The CR3BP has long attracted the Astrodynamics community since the times of Euler, given its rich and complex dynamics, yet extremely profitable for the mission design engineer [3]. While multi-body dynamics and the CR3BP may offer new interesting possibilities, old constraints still apply. This particularly holds for fuel optimization, which for deep-space probes becomes even of greater relevance as a fundamental performance barrier. When considering enhanced proximity operations, the design of robust GNC systems capable of performing fuel-optimal guidance and control in such a complex dynamics setting becomes a central problem to be solved.

Despite their complexity, the design of fuel-optimal solutions is a prominent problematic in space dynamics optimization since the times of the very foundation of modern Optimal Control Theory, as exemplified by the celebrated question by Edelbaum [4]. In fact, in the late 1960s, Primer Vector Theory (PVT) was born, as the result of the application of Pontryagin's Maximum Principle to the problem of impulsive space trajectory optimization. In this sense, the seminal work of Lawden, Neustadt, Potter, Prussing et al. [5–11], further revised in Section 3, remains as a solid foundation for the latest developments in the field, although numerical techniques are now predominant over analytical studies. Among the latter, Taheri and Saloglu [12, 13] have recently addressed Edelbaum's question via optimal switching surfaces, revealing the existence of iso-impulse rendezvous trajectories and re-interpreting the classical constraint on the primer vector norm as an opportunity, rather than optimality, condition. Bucchioni et al. [14] are investigating primer vector based strategies for impulsive transfer design in multi-body dynamics, following the work of Russel [15, 16] or Zhang et al. [17].

Specific effort has been dedicated over the last years to the development of new numerical solvers for general fuel-optimal orbital transfers, under the appropriate $\mathcal{L}_{1,p}$ fuel-consumption proxies [18], although solvers exist from the times of Lawden and Neustadt [19, 20]. From the numerical perspective, convex optimization and Model Predictive Control (MPC) are becoming standard technologies for general optimal control [21, 22], and may be found at the core of the most recently proposed algorithms, including those in this work. In fact, MPC already shows a plethora of applications and uses in the design of (sub)optimal rendezvous trajectories [23, 24]. Relevantly, Vazquez et al. have successfully proposed both, impulsive and continuous MPC schemes for constrained, robust close-range docking in Keplerian and NHRO scenarios [25–27], a path also explored by Cuevas el al. [2], Capannolo et al. [28] or Mammarella and co-authors [29]. Interestingly, attention is being currently drawn to the combination of Pontryagin's Principle and MPC, as given in Pagone et al. [30], with recent applications in multi-body dynamics rendezvous [31]. Arzelier, Claeys et al., in a prominent series of works, have explored different numerical recipes to solve the original Neustadt's problem of moments, all strongly founded on convex theory: in Kara-Zaïtri et al. and Arzelier et al. [32], polynomial optimization is used via convex relaxations (in the form of sum-of-squares optimization or a convergent hierarchy of linear matrix inequalities, respectively); an improved version of the algorithm, featuring mixed iterations, is presented in Arzelier et al. [33]; finally, convergent semi-infinite convex programming over discretized grids is leveraged in Arzelier et al. [34, 35]. Extensions of the above methods to constrained problems and formulations in the primal space are covered in Louembet [36]. Anagolously, Claeys et al. [37, 38] have exploited measures relaxations to obtain a hierarchy of semi-definite convex problems, in Linear Matrix Inequalities of reduced order. Koenig and D'Amico [39], similar to Gilbert [20], have also proposed a state-of-the-art solver, founded on convex reachable set theory, for the generalized fuel-optimal problem, in which the cost functional is time-varying. Their algorithm iteratively refines an estimate of the outward normal vector to the reachable set at the target state, which is equivalent to the classical primer vector optimality conditions. More recently, Foss and D'Amico extended previous results to control-bound optimal rendezvous problems [40]. Recent advances have led to the introduction of alternative solving strategies within space dynamics convex optimization, such as Alternating Direction Method of Multipliers (ADMM), as shown in Le Cleac'h and Manchester [41], the motivation behind this work; which also already shows relevant applications in combination with MPC schemes [42, 43].

In the spirit of the above literature review, this communications presents an integral suboptimal guidance-control scheme for (constrained) fuel-optimal rendezvous in the CR3BP. In particular, the solvers first presented in Cuevas et al. [44, 45] for the Keplerian setting are applied to fuel-optimal rendezvous in this new multi-body dynamics scenario. By profiting from the numerical performance of the solvers, as well as their closed, iterative form, we introduce a Pontryagin-based Model Predictive Control engine for suboptimal rendezvous. Ultimately, the local solution to the trajectory planning problem is found by simple iterations of proximal minimizations in approximate analytical form, without the need of any advanced numerical solver but an efficient system solver. This is achieved by fusing Alternating Direction Method of Multipliers (ADMM) with classical Primer Vectory Theory results. In particular, we address Neustadt's classical measure moment relaxation results [6] through the ADMM numerical paradigm, providing a really efficient indirect solver which does not suffer from the classical TBVP solver numerical instabilities. Via a classical time-shrinking MPC scheme, model discrepancies and uncertainties in the plant dynamics are allocated along the trajectory. The low footprint of the proposed algorithms and their straight, non-dedicated implementability make them a solid, certifiable candidate for real-time, embedded applications, providing suboptimal solutions at nearly null expenses. The proposed solvers are extensively deployed on several rendezvous practical missions to objectively assess their performance against fuel-optimal state-of-the-art techniques.

The remainder of this paper is organized as follows. Section 2 introduces the dynamical settings for the rest of the work, concerning mainly linear and nonlinear co-orbital dynamics in the CR3BP. In Section 3, the unconstrained and constrained versions of the minimum $\mathcal{L}_{1,p}$-norm optimal control problems are formalized, which proxy minimum fuel-consumption in Space Mechanics. Additionally, classical results from Primer Vector Theory are reviewed, upon which the numerical algorithms to be presented stand. Section 4 explores the mathematical framework exploited in the proposed solutions, where some fundamentals in the Theory of Proximal Operators and Alternating Direction Method of Multipliers (ADMM) are discussed. Section 5 details the numerical and computational, closed-form recursive solutions proposed to solve the original linear rendezvous problems, addressing both a direct and a moment-problem formulation of the former. To address the nonlinear nature of the CR3BP co-orbital dynamics, the proposed ADMM solver is embedded as the backbone guidance engine of shrinking-horizon scheme. Such Nonlinear Model Predictive Control (NMPC) loop, introduced in Section 6, allows to handle uncertainties while achieving suboptimal results. Section 7 provides several literature-standard, benchmark real-case mission scenarios to validate and verify the performance and design of the proposed trajectory optimization engine.

2 Co-orbital CR3BP dynamics

This paper is concerned with the design of optimal time-fixed rendezvous trajectories under co-orbital dynamics in the CR3BP. In this regime, the motion of the objects (namely, a target and a chaser spacecraft) are determined by their interaction with two Newtonian massive bodies. These are further assumed to revolve around each other on a circular Keplerian orbit, with mean motion ω. The osculating angular momentum vector and the revolving position of the smallest of the two bodies defines a synodic reference which co-rotates with the latter, see Fig. 1.

Moreover, it is customary to use dimensionless coordinates, such that the distance between the primaries is used as characteristic length and their orbital period around their common barycenter is taken as characteristic time. As a result, in these dimensionless coordinates, the primaries revolve at one radian per unit of dimensionless time; and, in the synodic reference frame, the position of the primaries is given by

$$\mathbf{R}_1 = -\mu\,\mathbf{i}\,, \quad \mathbf{R}_2 = (1-\mu)\,\mathbf{i}\,.$$

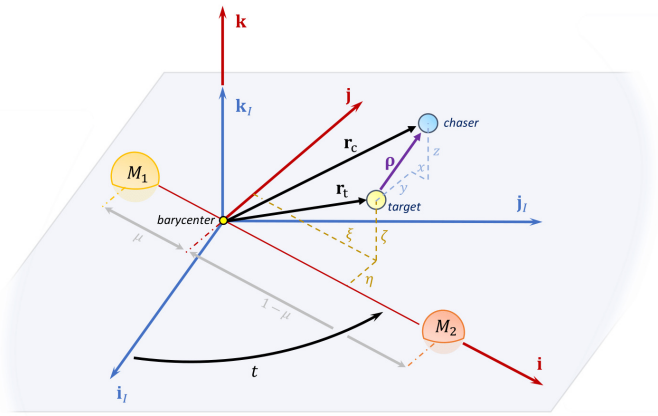

Fig. 1 Definition of the synodic frame.

In the above, μ is the normalised gravitational parameter of the orbit $M_2/(M_1+M_2)$, where M_i is the mass of the i-th primary. In this setup, the position vector of a spacecraft $\mathbf{r} = [\xi,\, \eta,\, \zeta]^\intercal$ evolves in time accordingly to

$$\begin{aligned}
\ddot{\xi} - 2\dot{\eta} - \xi &= -(1-\mu)\,\frac{\xi+\mu}{\|\mathbf{r}-\mathbf{R}_1\|^3} - \mu\,\frac{\xi-1+\mu}{\|\mathbf{r}-\mathbf{R}_2\|^3}\,,\\
\ddot{\eta} + 2\dot{\xi} - \eta &= -(1-\mu)\,\frac{\eta}{\|\mathbf{r}-\mathbf{R}_1\|^3} - \mu\,\frac{\eta}{\|\mathbf{r}-\mathbf{R}_2\|^3}\,,\\
\ddot{\zeta} &= -(1-\mu)\,\frac{\zeta}{\|\mathbf{r}-\mathbf{R}_1\|^3} - \mu\,\frac{\zeta}{\|\mathbf{r}-\mathbf{R}_2\|^3}\,.
\end{aligned} \tag{1}$$

Rendezvous between spacecraft is clearly a practical example of a Control Theory regulation problem: basically, it may be defined as making a spacecraft (the chaser) acquire the same position and velocity as a given reference (the target), which may be a physical or virtual object. Thus, rendezvous problems are intrinsically determined by the co-orbital motion between vehicles: that is, describing motion of one with respect to the other. Let us define the relative position vector $\boldsymbol{\rho}$ as

$$\boldsymbol{\rho} = x\,\mathbf{i} + y\,\mathbf{j} + z\,\mathbf{k} = \mathbf{r}_c - \mathbf{r}_t\,.$$

Here $\mathbf{r}_i$ stands for the synodic position vector of the target and chaser spacecraft; whose dynamics are ultimately described by Eq. (1). Let us also define the coordinates of $\mathbf{r}_t$ in the synodic frame as $\mathbf{r}_t = [\xi,\, \chi,\, \eta]^\intercal$.

When realized in the latter, the co-orbital state $\mathbf{s} = [\boldsymbol{\rho}^\intercal,\, \dot{\boldsymbol{\rho}}^\intercal]^\intercal$ between the target and the chaser is described by the following set of Hamiltonian nonlinear 2nd-order ODEs [46, 47]

$$\begin{aligned}
\ddot{x} - 2\dot{y} - x &= (1-\mu)\left(\frac{\xi+\mu}{\|\mathbf{r}_t-\mathbf{R}_1\|^3} - \frac{x+\xi+\mu}{\|\boldsymbol{\rho}+\mathbf{r}_t-\mathbf{R}_1\|^3}\right) + \mu\left(\frac{\xi-1+\mu}{\|\mathbf{r}_t-\mathbf{R}_2\|^3} - \frac{x+\xi-1+\mu}{\|\boldsymbol{\rho}+\mathbf{r}_t-\mathbf{R}_2\|^3}\right) + u_x,\\
\ddot{y} + 2\dot{x} - y &= (1-\mu)\left(\frac{\eta}{\|\mathbf{r}_t-\mathbf{R}_1\|^3} - \frac{y+\eta}{\|\boldsymbol{\rho}+\mathbf{r}_t-\mathbf{R}_1\|^3}\right) + \mu\left(\frac{\eta}{\|\mathbf{r}_t-\mathbf{R}_2\|^3} - \frac{y+\eta}{\|\boldsymbol{\rho}+\mathbf{r}_t-\mathbf{R}_2\|^3}\right) + u_y,\\
\ddot{z} &= (1-\mu)\left(\frac{\zeta}{\|\mathbf{r}_t-\mathbf{R}_1\|^3} - \frac{z+\zeta}{\|\boldsymbol{\rho}+\mathbf{r}_t-\mathbf{R}_1\|^3}\right) + \mu\left(\frac{\zeta}{\|\mathbf{r}_t-\mathbf{R}_2\|^3} - \frac{z+\zeta}{\|\boldsymbol{\rho}+\mathbf{r}_t-\mathbf{R}_2\|^3}\right) + u_z.
\end{aligned} \tag{2}$$

The control term $\mathbf{u}$ has been introduced already for future reference. This co-orbital CR3BP model exhibits rich dynamics, including both equilibrium points (rendezvous), bounded quasi-periodic motion and more complex structures, such as both hyperbolic and elliptic invariant manifolds [47].

As in classical Keplerian studies, retaining up to first order terms in Eq. (2) yields the Rendezvous Linear Model (RLM) [46, 47], which can be compactly expressed in matrix form as:

$$\dot{\mathbf{s}} = A(t)\,\mathbf{s} + B\,\mathbf{u} = \begin{bmatrix} \dot{\boldsymbol{\rho}} \\ \ddot{\boldsymbol{\rho}} \end{bmatrix} = \begin{pmatrix} 0_{3\times3} & I_{3\times3} \\ \Sigma(t) & \Omega \end{pmatrix} \begin{bmatrix} \boldsymbol{\rho} \\ \dot{\boldsymbol{\rho}} \end{bmatrix} + \begin{pmatrix} 0_{3\times3} \\ I_{3\times3} \end{pmatrix} \mathbf{u}\ ; \tag{3}$$

here $0_{3\times3}$ and $I_{3\times3}$ denote 3-dimensional null and identity matrices, respectively; the inertial term Ω reads as

$$\Omega = \begin{pmatrix} 0 & 2 & 0 \\ -2 & 0 & 0 \\ 0 & 0 & 0 \end{pmatrix}$$

and the Hessian matrix Σ can be computed following

$$\Sigma = -(\kappa_1 + \kappa_2)\, I_{3\times3} + 3\,\kappa_1\,(\mathbf{e}_1 \otimes \mathbf{e}_1) + 3\,\kappa_2\,(\mathbf{e}_2 \otimes \mathbf{e}_2),$$

where the operator $\otimes$ denotes the dyadic product, $\mathbf{e}_i$ are unit vectors pointing from the i-th primary to the target spacecraft, and the κ_i coefficients are defined as

$$\mathbf{e}_i = \frac{\mathbf{r}_\mathrm{t} - \mathbf{R}_i}{\|\mathbf{r}_\mathrm{t} - \mathbf{R}_i\|}\,, \quad \kappa_i = \frac{\mu_i}{\|\mathbf{r}_\mathrm{t} - \mathbf{R}_i\|^3}. \qquad i = 1, 2\,.$$

It is also common practice to describe the co-orbital state in a Local Vertical, Local Horizontal (LVLH) reference frame defined by the target's motion [31]. This introduces additional linear, inertial terms in Eq. (3), which derive from an additional Hamiltonian action. As a result, they are omitted for the sake of clarity, as they only complicate the definition of the state space matrix $A(t)$.

While the original RLM model is derived as a linearization of the true co-orbital dynamics around the target position vector, irrespectively of its natural motion, further simplification is possible if one considers it to orbit a libration point orbit (LPO). Precisely, in this work we exploit the Relative Libration Linear Model (RLLM), which considers co-orbital motion near the collinear libration points. In such cases, Σ is expected to become constant or (quasi-)periodic, respectively. Indeed, in this case it simplifies to [47]

$$\Sigma = \begin{pmatrix} 1 + 2\,c_2(\mu) & 0 & 0 \\ 0 & 1 - c_2(\mu) & 0 \\ 0 & 0 & -c_2(\mu) \end{pmatrix}. \tag{4}$$

The fundamental frequency c_2 depends on the libration point both spacecraft orbit, as well as on the gravitational mass parameter μ, as defined in Richardson [48]. As it can be seen, the co-orbital RLLM dynamics are therefore uncoupled from the exact chaser's and target's trajectories, providing an LTI dynamics model which will be useful in what follows.

3 Fuel-optimal time-fixed $\mathcal{L}_{1,p}$ Rendezvous Problem

As already explored, minimization of fuel consumption is a primary goal in space trajectory optimization. In general, such challenge is formally stated as an optimal control problem (OCP).

In particular, fuel consumption is proxied by exploiting the integral 1-norm of the p-norm of $\mathbf{u}$ as a valid running cost l_i, as advocated for in Ross [18]. Therefore, this work identifies a fuel-optimal rendezvous with the solution to the following Lagrange optimal control problem

Problem I. Unconstrained fuel-optimal rendezvous

$$\begin{aligned} \underset{\mathbf{u}\in\mathbb{U}}{\arg\min} \quad & J = \int_{t_0}^{t_f} \|\mathbf{u}(t)\|_p \, \mathrm{d}t \\ \text{subject to} \quad & \dot{\mathbf{s}} = A(t)\,\mathbf{s} + B(t)\,\mathbf{u} \,, \\ & (t_0, t_f) = (t^0, t^f) \,, \\ & \mathbf{s}(t_0) = \mathbf{s}_0 \,, \\ & \mathbf{s}(t_f) = \mathbf{0} \,. \end{aligned} \tag{5}$$

In the above, $\mathbf{s}$ describes the co-orbital state between the two spacecraft, being the state vector of the problem. Its first-order evolution with respect to the independent variable t is governed by linear applications $A(t) \in \mathbb{R}^{n\times n}$, $B(t) \in \mathbb{R}^{n\times m}$, as well as by the control vector field $\mathbf{u}$. The solution is given by the determination of the state-control trajectory $\{\mathbf{s}^*(t), \mathbf{u}^*(t)\}$ minimizing the cost functional J while satisfying the boundary conditions. The specific form of J identifies the control set $\mathbb{U}$ with the normed linear space of Lebesgue integrable functions $\mathbb{U} \subseteq \mathcal{L}_{1,p}\left([t_0, t_f], \mathbb{R}^m\right)$. Note that we consider only the time-fixed version of the rendezvous problem, in which the boundary clocks (t_0, t_f) are known a priori. The free version of the problem remains as an open line of research [49].

Depending on the exact spacecraft thruster configuration used in planning the rendezvous trajectory, different p-norms shall be used as proxies to fuel consumption. In fact, it can be shown that only the $p = 1, 2, \infty$ norms have physical significance when dealing with impulsive thrusting units [18], despite the common use of squared-integrable functions, denoted $\mathcal{L}_2$ (for which closed-form solutions exist, such as Kalman's Linear Quadratic Gaussian [50]). The former are defined as, for a vector $\mathbf{v} \in \mathbb{R}^n$,

$$\|\mathbf{v}\|_2 = \sqrt{\mathbf{v}^\intercal\,\mathbf{v}}\,, \quad \|\mathbf{v}\|_1 = \sum_{i=1}^{n} |v_i|\,, \quad \|\mathbf{v}\|_\infty = \max_{1\le i\le n} |v_i|\,.$$

In addition to Problem I, an explicit constraint on the control authority of the system is introduced through the action q-norm and the control bounds $u_{\min}, u_{\max} \in [0, \infty)$, to model hardware and operational limitations on the thrusters. Such constraint may also be used to promote control sparsity, which is again a desirable feature from both a hardware and operational perspective.

Problem II. Constrained fuel-optimal problem

$$\begin{aligned} \underset{\mathbf{u}}{\arg\min} \quad & J = \int_{t_0}^{t_f} \|\mathbf{u}(t)\|_p \, \mathrm{d}t \\ \text{subject to} \quad & \dot{\mathbf{s}} = A(t)\,\mathbf{s} + B(t)\,\mathbf{u} \,, \\ & \mathbf{s}(t_0) = \mathbf{s}_0 \,, \\ & \mathbf{s}(t_f) = \mathbf{0} \,, \\ & u_{\min} \le \|\mathbf{u}\|_q \le u_{\max} \,. \end{aligned} \tag{6}$$

Again, depending on the thruster configuration, different q-norms shall be used [18, 51], given by the dual norm of the selected fuel-consumption p-norm. Specifically, $p,\ q \in \mathbb{R} \times \{\infty\}$ are Hölder's conjugates

$$\frac{1}{p} + \frac{1}{q} = 1\,, \quad q = \frac{p}{p-1}.$$

3.1 Primer Vector Theory

After formalizing the fuel-optimal rendezvous problem, this Section reviews classical optimal impulsive control theory for linear systems, applied to in-space transport. This corpus of knowledge, known as Primer Vector Theory, is the theoretical foundation of the algorithms exploited in this work.

In the late 1960s, the foundational works of Lawden et al. [5, 8–10] in space trajectory optimization for impulsive probes led to the seminal Primer Vector Theory [52], which establishes the necessary conditions (NCs) for optimal transport within Newtonian gravity. For fixed-time linear settings, these become sufficient when strengthen with a continuous constraint [53]. The modern formal statement of the original Prussing-Clifton [53] necessary and sufficient conditions is due to Carter [54]. Obviously, such NCs arise as the result of the application of Pontryagin's Principle to the problem of optimal control in high-thrust, impulsive missions. Among others, practical applications of these NCs are, for example, the determination of optimal additional mid-course impulses to a given planned sequence to reduce fuel consumption [52].

Shortly after their presentation, the results by Lawden were rigorously confirmed by Neustadt in a series of works of primary importance [6, 55]. These relied on duality theory and functional analysis, founding the solution to Problem I through a relaxation argument in an augmented dual control space $C^\star$. First, Problem I is transformed into a moment problem. In order to so, the state trajectory $\mathbf{s}(t)$ is initially expressed via Lagrange's formula

$$\mathbf{s}(t) = \Phi(t, t_0)\,\mathbf{s}_0 + \int_{t_0}^{t} \Phi(t, \tau)\,B(\tau)\,\mathbf{u}(\tau)\,\mathrm{d}\tau\ .$$

In here, Φ is again the State Transition Matrix of the system. For linear time-varying dynamics, as already seen, this may be expressed as a function of the fundamental matrix of the system $\phi(t)$

$$\Phi(t, t_0) = \phi(t)\,\phi^{-1}(t_0)\ .$$

Defining $Y = \phi^{-1}(t)\,B(t)$, Lagrange's formula may be arranged as

$$\mathbf{c} = \phi^{-1}(t_f)\,\mathbf{s}(t_f) - \phi^{-1}(t_0)\,\mathbf{s}(t_0) = \int_{t_0}^{t_f} Y(\tau)\,\mathbf{u}(\tau)\,\mathrm{d}\tau\ .$$

Thus, assuming the elements of $Y(t) = [\mathbf{y}_1(t), \mathbf{y}_2(t), ...\mathbf{y}_n(t)]^\intercal$ are linearly independent –the system is normal–, Problem I is transformed into

Problem III. Minimum Norm Moment Problem

$$\begin{aligned} \inf_{\mathbf{u}\,\in\,\mathcal{L}_{1,p}([t_0,t_f],\mathbb{R}^r)} \quad & \|\mathbf{u}\|_{1,p} = \int_{t_0}^{t_f} \|\mathbf{u}(t)\|_p\,\mathrm{d}t \\ \text{subject to} \quad & \mathbf{c} = \int_{t_0}^{t_f} Y(\tau)\,\mathbf{u}(\tau)\,\mathrm{d}\tau\ . \end{aligned} \tag{7}$$

Through duality arguments [6], Neustadt arrives at the following equivalent Semi-Infinite Convex Optimization Problem (SICP) in the finite vector $\boldsymbol{\lambda} \in \mathbb{R}^n$.

Problem IV. SICP Problem

$$\begin{aligned} \min_{\boldsymbol{\lambda}\in\mathbb{R}^n} \quad & \boldsymbol{\eta} = -\mathbf{c}^\intercal\boldsymbol{\lambda} \\ \text{subject to} \quad & \|Y^\intercal(t)\boldsymbol{\lambda}\|_q \le 1\ . \end{aligned} \tag{8}$$

The optimal control law is then recovered from $\boldsymbol{\lambda}$ through Theorem 1

Theorem 1 *Let* $\mathbf{y}_i \in C([t_0, t_f], \mathbb{R}^m)$, $i = 1, ..., n$ *and* $\boldsymbol{\lambda} \in \mathbb{R}^n$ *be a solution to Problem IV. Define the set* $\Gamma = \{t \in [t_0, t_f],\ \|\mathbf{y}(t)\|_q = \max_{t_0 \le t \le t_f} \|\mathbf{y}(t)\|_q = 1\}$.

There is an optimal solution $\mathbf{u}^*$ *of the relaxed Problem III, which is a step function with at most n points of discontinuity,* $\bar{\theta}_j \in \Gamma$, $j = 1, ..., N \le n$.

The complete proof may be found in the original Neustadt [6]. Theorem 1 shows that the optimal control trajectory is impulsive: the relaxed solution converges to a linear combination of Dirac delta measures. Moreover, the optimal number of impulses N^* is actually upper-bounded by the dimension n of the fixed final conditions of the problem. In short, the optimal control problem basically consists of finding the at maximum N^* impulses $\{\Delta V(t_i)\}_{i=1,2,...,N^*}$ and their locations $\{t_i\}_{i=1,2,...,N^*}$ to satisfy the boundary condition

$$\mathbf{c} = \sum_{i=1}^{N^*} Y(t_i)\, \Delta V(t_i)\ .$$

In fact, the vector $\mathbf{p}(t) = Y^\intercal(t)\, \boldsymbol{\lambda}$ is nothing but Lawden's Primer Vector, the adjoint of the velocity vector $\boldsymbol{\lambda}_v$

$$\mathbf{p}(t) = -\boldsymbol{\lambda}_v\ ,$$

which also satisfies the same dynamics as the system state $\mathbf{s}$

$$\begin{bmatrix} \mathbf{p} \\ \dot{\mathbf{p}} \end{bmatrix} = \Phi(t, t_0) \begin{bmatrix} \mathbf{p}_0 \\ \dot{\mathbf{p}}_0 \end{bmatrix}\ .$$

Moreover, the magnitudes ΔV_i of the impulses admit the interpretation of the Lagrange multipliers associated to the infinite constraint $\|\mathbf{p}\|_q \le 1$ [6], while $\boldsymbol{\eta}$ is directly the optimal fuel consumption [32, 56].

The following Section addresses modern optimization techniques to solve Problems II and IV efficiently from the perspective of convex optimization.

4 Proximal Operators and Alternating Direction Method of Multipliers

In [45], Alternating Direction Method of Multipliers (ADMM) is exploited to its full potential to present closed-form, algorithmic solutions to the general $\mathcal{L}_{1,p}$-regulation problems. The resulting algorithms are here employed to solve in a cost-efficient manner CR3BP rendezvous problems. For the sake of completeness, ADMM is overviewed in this Section.

ADMM is an algorithm intended to blend the decomposability of dual ascent with the superior convergence properties of the method of multipliers, and is highly used as general convex optimization technique [57]. It was first proposed by Gabay, Mercier, Glowinski and Marrocco in 1976 [58, 59] and shows a wide variety of applications across disciplines, from Machine Learning to resource allocation problems.

ADMM, as an operator splitting algorithm, takes the form of a decomposition-coordination procedure, in which the solutions to small local subproblems are coordinated to find a solution to the large global, original problem. This allows to blend the benefits of the classical optimization techniques of dual decomposition and augmented Lagrangian methods for constrained optimization.

Consider the following optimization problem

$$\begin{aligned} \underset{\mathbf{x},\,\mathbf{z}}{\arg\min} \quad & f(\mathbf{x}) + g(\mathbf{z})\,, \\ \text{subject to} \quad & A\mathbf{x} - B\mathbf{z} = \mathbf{c}\,, \end{aligned} \tag{9}$$

in which the cost functions f and g are separable in their arguments, and with primal variables $\mathbf{x}$, $\mathbf{z}$ and dual $\mathbf{y}$. The ADMM solution algorithm consists in performing the following iterates to minimize the problem's Lagrangian L of interest

$$\mathbf{x}^{k+1} = \underset{\mathbf{x}}{\arg\min}\, L_\rho\left(\mathbf{x},\, \mathbf{z}^k,\, \mathbf{y}^k\right)\,, \tag{10a}$$

$$\mathbf{z}^{k+1} = \underset{\mathbf{z}}{\arg\min}\, L_\rho\left(\mathbf{x}^{k+1},\, \mathbf{z},\, \mathbf{y}^k\right)\,, \tag{10b}$$

$$\mathbf{y}^{k+1} = \mathbf{y}^k + \left(A\,\mathbf{x}^{k+1} - B\,\mathbf{z}^{k+1} - \mathbf{c}\right)\,. \tag{10c}$$

The iterates are finished under appropriate terminating conditions for both the primal and dual residuals, which are discussed in-depth in Boyd [57].

The most fundamental convergence results for ADMM apply under the following two assumptions:

1) f and g are closed, proper, and convex; their epigraphs are closed nonempty convex sets. Assumption 1 implies that the subproblems embedded in the $\mathbf{x}$ and $\mathbf{z}$-updates are solvable on their own.
2) Strong duality holds; the un-augmented Lagrangian has a saddle point.

If the above two apply, the ADMM iterates satisfy the following

1) Residual convergence: $A\,\mathbf{x}^k - B\,\mathbf{z}^k - \mathbf{c} = \mathbf{r}^k \to \mathbf{0}$ as $k \to \infty$; the iterates approach feasibility.
2) Objective convergence: $f(\mathbf{x}^k) + g(\mathbf{z}^k) \to J^+$ as $k \to \infty$, the objective function of the iterates approaches the optimal value.

It shall be stated that in general, primal feasibility is not guaranteed: $\mathbf{x}^k$ and $\mathbf{z}^k$ do not approach the optimal point. In practice, ADMM will be mostly useful in cases when modest accuracy is sufficient, even whenever one of the two assumptions do not hold. Moreover, ADMM will converge even when the minimization steps are not carried out exactly [60]. This result is of interest in situations where the variable updates are completed or embedded into an iterative method –such as within the guidance core in Model Predictive Control, as in this work.

The latter is concerned with optimization problems for which the following trivial consensus equation holds

$$\mathbf{x} - \mathbf{z} = \mathbf{0}\,.$$

This simplified form of the general ADMM Eq. (10c) leads to $\mathbf{x}$ and $\mathbf{z}$ minimizations of the form

$$\mathbf{x}^+ = \underset{\mathbf{x}}{\arg\min}\left(f(\mathbf{x}) + (\rho/2)\,\|\mathbf{x} - \mathbf{v}\|_2^2\right)\,,$$

$$\mathbf{z}^+ = \underset{\mathbf{z}}{\arg\min}\left(g(\mathbf{z}) + (\rho/2)\,\|\mathbf{z} - \mathbf{w}\|_2^2\right)\,.$$

which, for closed convex f and g, are identified as proximal operators [61], denoted $\text{prox}_{f,\,\rho}\,\mathbf{v}$ and $\text{prox}_{g,\,\rho}\,\mathbf{w}$. The $\mathbf{x}$-minimization in the proximity operator is generally referred to as proximal minimization. While proximal operators admit several interpretations, they may be understood as a regularized projection, which minimizes f as long as $\mathbf{x}$ stays close to $\mathbf{v}$ in a convex sense. Proximal operators offer the advantage of presenting simple, closed-form, in may cases involving only modular-arithmetic operations; which is of interest for online optimization and guidance.

5 Optimal linear ADMM regulation for $\mathcal{L}_{1,p}$ fuel problems

Building on the previous both theoretical and practical results, Problems II and IV are solved in this Section in closed-form via the application of ADMM. For an in-depth overview of the methods, the reader is referred to Cuevas et al. [45], where the solvers are first introduced for Keplerian rendezvous problems.

5.1 Neustadt solver: ADMM solution to Problem IV

Given its simplicity and the availability of modern, efficient numerical solvers, the original SICP optimization Problem (IV) by Neustadt has received great attention in recent years as a cost-effective, practical method for optimal rendezvous planning [34]. Its general formulation, independent of the p-norm used, is also readily oriented towards its practical implementation when compared to other formulations of Problem I. This Section develops the ADMM solution for such problem.

Problem IV is already in the form of a consensus, separable problem, as needed by the ADMM. In particular, identifying $\boldsymbol{\lambda}$ in Problem IV with our decision vector $\mathbf{x} \in \mathbb{R}^n$, $n = 6$, the problem's cost function is

$$J = -\mathbf{c}^\intercal \mathbf{x} + \mathcal{I}_C(\mathbf{x}), \quad C = \{\mathbf{x} \in \mathbb{R}^n \mid \|Y^\intercal(t)\,\mathbf{x}\|_q \leq 1\}. \tag{11}$$

In short, Neustadt's problem is equivalent to the following optimization on the convex, closed, non-empty cone $\mathcal{K}$ [57]

$$\begin{aligned} &\min && J = -\mathbf{c}^\intercal \boldsymbol{\lambda} \\ &\text{subject to} && \boldsymbol{\lambda} \in \mathcal{K}, \quad \mathcal{K} = \{\boldsymbol{\lambda} \in \mathbb{R}^6 \mid \|Y(t)^\intercal \boldsymbol{\lambda}\|_q \leq 1, -\mathbf{c}^\intercal \boldsymbol{\lambda} \leq 0\}. \end{aligned}$$

In particular, the cone $\mathcal{K}$ does not only constrain the primer vector to lie on the celebrated unit q-ball, but also restricts $\boldsymbol{\lambda}$ to belong to the halfspace $\mathcal{H}$

$$\mathcal{H} = \{\boldsymbol{\lambda} \in \mathbb{R}^n \mid -\mathbf{c}^\intercal \boldsymbol{\lambda} \leq 0\}.$$

The rationale behind such projection lies in the physical significance of the cost function f as the negative of a fuel consumption metric, which therefore cannot be positive.

While the problem is only in $\boldsymbol{\lambda}$, to allow a closed-form solution, the decision vectors $\mathbf{z}$, $\mathbf{x} \in \mathbb{R}^n$ and dual variables $\mathbf{y}$ are augmented to include the primer vectors at the specified time grid $\mathcal{T}$, leading to the partitions

$$\mathbf{X} = \begin{bmatrix} \boldsymbol{\lambda}_x \\ \mathbf{p}_1^x \\ \vdots \\ \mathbf{p}_N^x \end{bmatrix} \in \mathbb{R}^{n+3N}, \quad \mathbf{Z} = \begin{bmatrix} \boldsymbol{\lambda}_z \\ \mathbf{p}_1^z \\ \vdots \\ \mathbf{p}_N^z \end{bmatrix} \in \mathbb{R}^{n+3N}, \quad \mathbf{Y} = \begin{bmatrix} \boldsymbol{\lambda}_y \\ \mathbf{p}_1^y \\ \vdots \\ \mathbf{p}_N^y \end{bmatrix} \in \mathbb{R}^{n+3N}$$

As such, the miss-vector $\mathbf{c} \in \mathbb{R}^n$ is augmented to be

$$\mathbf{C} = \begin{bmatrix} -\mathbf{c} \\ \mathbf{0} \end{bmatrix} \in \mathbb{R}^{n+3N}.$$

Once this is done, the ADMM solution can be shown to be, at the k-th iteration,

Pure ADMM solution for Problem IV

$$\mathbf{X}^{k+1} = \pi\left(A,\, \mathbf{b}\right)\,, \tag{12a}$$

$$\mathbf{p}_i^{z,k+1} = \Pi_C\left(\mathbf{p}_i^{x,k+1} + \mathbf{p}_i^{y,k}\right), \quad i = 1, ..., N\,, \tag{12b}$$

$$\boldsymbol{\lambda}_z^{k+1} = \left(\boldsymbol{\lambda}_x^{k+1} + \boldsymbol{\lambda}_y^{k}\right) - \max\left\{\mathbf{c}^\top\left(\boldsymbol{\lambda}_x^{k+1} + \boldsymbol{\lambda}_y^{k}\right), 0\right\}\frac{\mathbf{c}}{\|\mathbf{c}\|_2^2}\,, \tag{12c}$$

$$\mathbf{Y}^{k+1} = \mathbf{Y}^{k} + \mathbf{X}^{k+1} - \mathbf{Z}^{k+1}\,. \tag{12d}$$

The $\mathbf{X}$-update is ruled by minimizing a linear programming cost function on a convex set

$$\mathbf{X} = \arg\min f(\mathbf{X}) = \mathbf{C}^\top \boldsymbol{X}\,, \quad \mathrm{dom}(f) = \{\mathbf{X} \in \mathbb{R}^{n+3N} \;\mid\; A\mathbf{X} = \mathbf{b}\}\,.$$

This is defined as the solution of the following Karush-Kuhn-Tucker system $\pi\left(A, \mathbf{b}\right)$ [57]

$$\begin{pmatrix} \rho I & P^\top \\ P & 0 \end{pmatrix}\begin{bmatrix} \mathbf{X}^{k+1} \\ \boldsymbol{\nu} \end{bmatrix} = \begin{bmatrix} \mathbf{C} + \rho\left(\mathbf{Z}^k - \mathbf{Y}^k\right) \\ \mathbf{0} \end{bmatrix}\,.$$

The matrix block P defines the linear relationship between the primer vector $\mathbf{p}$ and $\boldsymbol{\lambda}$

$$\mathbf{p}(t) = Y^\top(t)\,\boldsymbol{\lambda}\,,$$

which may be expressed as

$$\begin{pmatrix} Y^\top(t_i) & -I_{3\times 3} \end{pmatrix}\begin{bmatrix} \boldsymbol{\lambda} \\ \mathbf{p}(t_i) \end{bmatrix} = \mathbf{0}\,.$$

When considering the complete time grid $\{t_i\}$, the linear matrix $P \in \mathbb{R}^{3N\times(n+3N)}$ results in

$$P = \begin{pmatrix} \mathrm{ver}\left\{Y^\top(t_i)\right\}_{i=1}^N & I_{N\times N} \otimes -I_{3\times 3} \end{pmatrix}\,,$$

where the operator $\otimes$ denotes Kronecker's tensor product.

The $\mathbf{z}$-update is partitioned for both the primer vectors $\mathbf{p}_i^z$ and $\boldsymbol{\lambda}_z$: for the former, projection onto the unit q-norm ball C is needed, all of which may be found in the above optimizations; in the latter case, $\boldsymbol{\lambda}_z$ is projected on the halfspace $\mathcal{H}$.

Once the solution $(\{\mathbf{p_i}\}, \boldsymbol{\lambda})$ is recovered, the optimal control plan $\{(t_i, \mathbf{u}_i)\}$ is solved for via solving the following linear system

$$\mathbf{c} = \sum_{i=1}^{L} Y(t_i)\,\mathbf{u}_i\,. \tag{13}$$

The number of impulses L together with their location $\{t_i\}$ are determined from the primer vector sequence $\{\mathbf{p}_i\}$ [34, 35]

$$\{t_i\} = \{\, t \in \mathcal{T} \;\mid\; \|Y(t_i)\,\boldsymbol{\lambda}\|_q = 1\}\,, \quad L = \mathrm{card}\,\{t_i\}\,.$$

Whenever $L > m$, the impulses set is pruned so that Eq. (13) is solved for just m impulses (the sequence $\{\mathbf{u}_i\}$ is not linearly independent).

To robustify its performance, the numerical implementation of the algorithm is further embedded into a sequence of discrete problems, following the ideas of Arzelier et al. [34], Koenig et al. [39] and Foss and D'Amico [40]. Consider a global discretization $\mathcal{T}^G = \{t_i\}_{i=0}^N$. A second, iteration-dependent discretization grid is initialized with $\mathcal{T}^0 = \{t_0, t_{N/2}, t_N\}$. At each iteration, new impulsive locations are

added, based on maximization of the q-norm of the resulting primer vector over the global mesh $\mathcal{T}^G$.

$$\mathcal{T}^{k+1} \leftarrow \mathcal{T}^k \cup \{t_i \in \mathcal{T}^G \mid \arg\max \|Y^\intercal(t_i)\,\boldsymbol{\lambda}^k\|_q\}\,.$$

Moreover, the discretization grid $\mathcal{T}^{k+1}$ is pruned of those epochs at which the primer vector norm cannot reach the switching function

$$\mathcal{T}^{k+1} \leftarrow \{t_i \in \mathcal{T}^{k+1} \mid \|Y^\intercal(t_i)\,\boldsymbol{\lambda}^k\|_q > 1-\epsilon\}\,.$$

Finally, the ADMM iterates solution of the k-th problem is considered feasible if the following condition holds

$$\max \|Y^\intercal(t_i)\,\boldsymbol{\lambda}^k\|_q < 1+\epsilon\,, \quad t_i \in \mathcal{T}^k\,,$$

for a user-specified numerical tolerance ϵ. The algorithm also terminates if $\mathcal{T}^K = \emptyset$. The complete Neustadt-ADMM procedure is shown in Algorithm 1.

Algorithm 1: Neustadt-ADMM solver

Data: N, p, $\mathcal{T}^G$, $Y^\intercal(t_i)$, $\mathbf{c}$, ϵ
Result: $\{(t_i, \Delta\mathbf{V}_i)\}_{i=1,\dots,L}$
$k = 0$
$\mathcal{T}^0$ $\boldsymbol{\lambda}_x^0$, $\boldsymbol{p}(t_i)_z^0 = \mathbf{0}$
while $max\,\|Y^\intercal(t_i)\,\boldsymbol{\lambda}_x^k\|_q > 1+\epsilon$ **do**
  $\boldsymbol{\lambda}_x^{k+1} \leftarrow \text{ADMM}\left(\mathcal{T}^k, Y(t_i), \mathbf{c}\right)$
  $\mathcal{T}^{k+1} \leftarrow \mathcal{T}^k$
  $k = k+1$
end
$L = \text{card}\,\mathcal{T}$
$\mathbf{p}_i = Y^\intercal(t_i)\,\boldsymbol{\lambda}_x^k$
$\{\Delta\mathbf{V}_i\} \mid \mathbf{c} = \sum_{i=1}^{L} Y(t_i)\,\Delta\mathbf{V}_i$

5.2 Primal solver: ADMM solution for direct l_p-optimization

While Neustadt solver offers a practical closed-form algorithm for unconstrained rendezvous optimization, it is not able to handle constrained problems instead. Thus, we may also introduce a direct or primal solver to target such set of problems.

Again, Problem II realized for an l_p-norm reads as follows

$$\begin{aligned}
\underset{\mathbf{u}\in\mathbb{U}}{\arg\min} \quad & J = \sum_{i=1}^{N} \|\mathbf{u}(t)\|_p \\
\text{subject to} \quad & \dot{\mathbf{s}} = A(t)\,\mathbf{s} + B(t)\,\mathbf{u}\,, \\
& \mathbf{s}(t_0) = \mathbf{s}_0\,, \\
& \mathbf{s}(t_f) = \mathbf{0}\,, \\
& u_{\min} \le \|\mathbf{u}\|_q \le u_{\max}\,.
\end{aligned}$$

To exploit the ADMM algorithm, a separable form of the problem is proposed

$$\begin{aligned} \underset{\mathbf{x},\,\mathbf{z}}{\arg\min} \quad & f(\mathbf{x}) + g(\mathbf{z})\,, \\ \text{subject to} \quad & \mathbf{X} - \mathbf{Z} = \mathbf{0}\,, \\ & f(\mathbf{x}) = \mathcal{I}_C\,(\mathbf{X})\,, \\ & g(\mathbf{z}) = \sum_{i=1}^{N} \|\mathbf{z}_i\|_p + \mathcal{I}_{\mathcal{B}}\,(\mathbf{z}_i)\,, \quad i = 1, 2, ..., N\,. \end{aligned} \tag{14}$$

In this case, f represents the indicator function of the flow map set $C = \{\mathbf{X} \in \mathrm{R}^{3N} \,|\, \hat{\Phi}\,\mathbf{X} = \mathbf{s}_f - \Phi(t_f, t_0)\,\mathbf{s}_0\}$. Here $\hat{\Phi}$ is given by the horizontal concatenation of the STM evaluated at the impulsive times, namely

$$\hat{\Phi} = \mathrm{hor}\,\left\{\Phi(t_f, t_i)\,B(t_i)\right\}, \quad i = 1, 2, ..., N\,.$$

On the other hand, g both penalizes fuel consumption and constrains the impulses to lie on a ball of maximum radius $u_{\max}$, $\mathcal{B} = \{\mathbf{z} \in \mathbb{R}^3 \,|\, 0 \leq \|\mathbf{z}_i\|_q \leq u_{\max}\}$. The solution to problem Eq. (14) is given by the iteration of the following system of proximal minimizations:

Primal ADMM solver for the l_p fuel-optimal problem

$$\mathbf{X}^{k+1} = \left(I - \hat{\Phi}^{\dagger}\hat{\Phi}\right)(\mathbf{Z}^k - \mathbf{Y}^k) + \hat{\Phi}^{\dagger}\left[\mathbf{s}_f - \Phi(t_f, t_0)\,\mathbf{s}_0\right]\,, \tag{15a}$$

$$\mathbf{z}_i^{k+1} = \mathcal{S}_p\left(\rho, \mathbf{x}_i^{k+1} + \mathbf{y}_i^k\right)\,, \quad i = 1, 2, ..., N\,. \tag{15b}$$

$$\mathbf{z}_i^{k+1} = \Pi_q\left(u_{\max}, \mathbf{z}_i^{k+1}\right)\,, \quad i = 1, 2, ..., N\,. \tag{15c}$$

$$\mathbf{Y}^{k+1} = \mathbf{Y}^k + \mathbf{X}^{k+1} - \mathbf{Z}^{k+1}\,, \quad i = 1, 2, ..., N\,. \tag{15d}$$

The first update is the projection of $\mathbf{X}$ on the convex set $A\mathbf{X} = \mathbf{b}$. The update of Z is performed block-wise and is decomposed in two consecutive steps: 1) first, the ρ-weighted proximal minimization of the p-norm, such as the block soft-thresholding operator in the l_2 case [61], is applied to promote fuel minimization via the operator $\mathcal{S}_p(\rho, \cdot)$; 2) the resulting impulse sequence $\{\mathbf{z}_i\}$ is constrained to lie on the unit q-norm ball $\mathcal{B}$ by means of the projection operator $\Pi_q(\cdot)$. Because both all vector norms and the set $\mathcal{B}$ are convex, the algorithm shows dual convergence, and both primal and dual feasibility (in both $\mathbf{Z}^{k+1}$ and $\mathbf{X}^{k+1}$). Notice that the direct solution to Problem I is just given by eliminating the second step in the proximal operator in $\mathbf{Z}$.

5.3 Discussion on the solvers

Up to now, despite their efficiency, specialized solvers have been needed to address the semi-infinite convex nature of Problem IV, given by the q-norm constraint on the primer vector. However, our ADMM solution proposes a simple, iterative solution in need only of extremely simple arithmetic operations, an interesting feature for its use in embedded firmware. Moreover, given its convex quadratic form, both primal and dual infeasibility certificates are easily amenable [62], augmenting the robustness of the method for their real-time implementation. In addition, the method does not require any initial guess or sequence of increasingly complex problems, as in state-of- the-art solvers [34, 39]. Yet it requires the heuristic selection of the penalty parameter ρ.

In comparison, the primal solver is the most general one, able to handle both Problem I and II, and may be further modified to include any additional constraints on the problem. However, it does not directly address any optimality condition, for which Neustadt solution is aimed. Note that technically speaking, the control-bound constraint in Problem II directly precludes the solution to be generalized by

a Dirac's comb –delta measures require of *infinite* amplitudes–, thus ruling out the possibility of using Neustadt solver.

6 Optimal nonlinear regulation through MPC-ADMM

The presented guidance, trajectory planning techniques presented benefit from surrogate relative motion models when addressing the regulation problem at hands, mainly based on an appropriate linearization of true nonlinear dynamics and the corresponding STM $\Phi(t, t_0)$. Therefore, any control policy $\mathbf{\Pi}(t)$ computed under such dynamics is not guaranteed to regulate the relative state vector under the true nonlinear field. In general, some form of feedback is needed to successively refined $\mathbf{\Pi}(t)$ to comply with the nonlinear relative motion dynamics and the true performance of the GNC system as a whole. Such feedback loop may be implemented online through Model Predictive Control (MPC), as described now.

MPC is an optimal control technique based on iterative optimization, introduced in the late 1980s [63, 64], which shows a long tradition within rendezvous and proximity operations studies [2, 23, 24, 26, 27, 65, 66]. In the MPC paradigm, an optimal surrogate guidance problem is solved for a given prediction time horizon $t_i = 0, 1, ..., T$; and as a result, both a state trajectory $\{\mathbf{s}_i(t_i)\} = \mathbf{s}_1, \mathbf{s}_2, ..., \mathbf{s}_T$ and control action policy $\{\mathbf{U}_i(t_i)\} = \mathbf{U}_1, \mathbf{U}_2, ..., \mathbf{U}_T$ are returned. The controller executes the actions $\mathbf{U}_1$, and, after the plant natural rollout ahead, the optimization problem is run again with the time horizon receded $t_i = 0, 1, ..., T-1$. In this way, the true nonlinearities and unmodelled uncertainties in the surrogate guidance model are accommodated through a time-shrinking horizon scheme under the true plant dynamics. Under perfect modelling of the dynamics, the scheme reproduces an optimal path under Bellman's Principle of Optimality; in our case, we target suboptimal performance at the expense of close-loop behavior. MPC can be understood as a practical application of the more general Real Time Optimal Control (RTOC), which has long elucidated practical aerospace applications. In a broader sense, RTOC is comprised with the 'instantaneous' availability of optimal control laws, which, when generated at a given frequency with updated state estimates, manage uncertainty within the plant through a close-loop action [50, 67]. It shall be noticed that orbital motion is particularly well-suited for MPC deployments [24], as the typical time scales may be considered to be slow when compared to the computational time required to complete the inner optimization.

In our specific setting, the inner optimization at each MPC epoch is run via the presented solvers, leading to a very lightweight, Pontryagin-based online guidance-control system. The trade-off is, of course, the loss of certified optimality of the overall solution.

Within the MPC scheme, and to accelerate convergence, the ADMM solution $\mathbf{x}_k^*$, $\mathbf{z}_k^*$ and $\mathbf{y}_k^*$ at time T_i is used as an initial guess for the optimization at the next time step T_{i+1}. For the initial optimization at epoch 0, the decision and dual vectors are always initialized to be null vectors $\mathbf{0}$ of appropriate dimension, which corresponds to a coasting solution. Based on current state estimates[1], linearization of the state model is achieved if needed –for example, when using the RLM within the solvers– and the STM re-computed along the linearized trajectory. For embedded applications, this scheme can be easily implemented following Real-Time Iteration MPC for enhanced performance [68].

7 Applications and mission cases

The performance of the solvers will be demonstrated in two practical rendezvous mission scenarios: first, the algorithms are numerically compared against a state-of-the-art SICP solver, presented in Serra

[1]The impact of state estimation is not considered in this work.

et al. [35]. Once done, the optimization of a realistic, Earth-Moon halo orbit rendezvous mission is presented to demonstrate the close-loop capabilities of the design.

7.1 Numerical implementation and setup

Before introducing the concrete practical examples, the numerical implementation of the solutions shall be briefly overviewed.

The two solvers have been implemented following an object-oriented methodology in Matlab 2021b [69]. Numerical integration of the co-orbital and absolute motion dynamical systems is achieved through a variable-step, variable-order Adams–Bashforth–Moulton predictor–corrector solver of orders 1 to 13, which benefit from error estimation and local extrapolation for enhanced accuracy. Such an integrator has been commercially implemented in the same Matlab 2021b (ode113). The same integrator is used to compute the STM along a given reference trajectory when using linear time-varying co-orbital models; otherwise, matrix exponentials are used to pre-compute the STM.

As already indicated, the implementation of the ADMM solver follows the discussion in Boyd [57]; moreover, Neustadt solver is constructed upon a modified version of the open-source solver OSQP, which directly targets general convex quadratic programs [70].

Termination conditions are given by the l_2-norms of the primal $\mathbf{r}^k$ and dual $\mathbf{s}^k$ residuals [57]

$$\mathbf{r}^k = \left(A\mathbf{x}^k - B\mathbf{z}^k - \mathbf{c}\right) \in \mathbb{R}^n\,, \quad \mathbf{s}^{k+1} = \rho A^\intercal B\left(\mathbf{z}^{k+1} - \mathbf{z}^k\right) \in \mathbb{R}^p\,;$$

in particular, the following conditions are used

$$\|\mathbf{r}^k\|_2 \leq \sqrt{n}\,\epsilon_{\text{abs}} + \epsilon_{\text{rel}} \max\left(\|A\mathbf{x}^k\|_2, \|B\mathbf{z}^k\|_2, \|\mathbf{c}\|_2\right)\,,$$
$$\|\mathbf{s}^k\|_2 \leq \sqrt{n}\,\epsilon_{\text{abs}} + \epsilon_{\text{rel}}\,\|A^\intercal\mathbf{y}^k\|_2\,.$$

The relative tolerance ϵ_{rel} are all set to $1\cdot10^{-6}$ in the examples, while for in the absolute case, ϵ_{abs} depends on the typical scale of the problem, ranging from $1\cdot10^{-5}$ for dimensional problems to $1\cdot10^{-9}$ when using canonical units. In addition, the algorithms are also upper-bounded by a user-selected maximum number of iterations. For Neustadt solver, the tolerance hyperparameters are selected to be $\epsilon_1 = 1\cdot10^{-5}$.

Finally, all simulations were performed using an 11th Gen Intel(R) Core(TM) i7-1165G7 @ 2.80GHz with 15.7 GB of RAM. Results in all cases are provided in an average sense over 25 iterations of the solution process.

7.2 Comparison against a state-of-the-art SICP solver

The mission scenario implies the rendezvous of two probes in the vecinities of the L_2 point in the Earth-Moon system. As a result, the linear dynamical model employed is the RLLM, with the parameter c_2 equal to $c_2 = 3.190425213622208$.

The initial and final co-orbital conditions of the rendezvous are given by –in dimensional S.I. units–

$$\mathbf{s}(t_0) = \begin{bmatrix}6449.40 & 65117.03 & 22814.91 & -0.0312 & 0.0392 & 0.2114\end{bmatrix}^\intercal\,,$$
$$\mathbf{s}(t_f) = \begin{bmatrix}59066.09 & 67728.64 & 84015.47 & -0.1087 & 0.1616 & -0.1730\end{bmatrix}^\intercal\,.$$

The existence of an energy-integral in the CR3BP –known as the Jacobi constant [2]– allow us to establish the minimum l_2 ΔV-requirement to accomplish the transfer/bridge the energy gap between

the two initial conditions in an l_2-sense. In non-dimensional units, this corresponds to a minimum of $\Delta V_{\text{min}} = 0.2734$ m/s.

Both the fuel-optimal problem is solved for the $p = 1, 2$ proxies. A total number of $N = 100$ impulsive locations is selected to define $\mathcal{T}^G$. This will put into manifest the performance of the solver even in very low-resolution scenarios. The corresponding results are shown next in Table 1 and Table 2, which compare them against those in Serra et al. [35].

Table 1 Trajectory optimization results for Scenario I, $p = 1$.

	Neustadt Solver	**Direct Solver**	**Serra et al. [35]**
N	100	100	1000
ρ	$N^{-3/2}$	N	N/A
N^*	4	4	4
$\boldsymbol{\lambda}$	$\begin{bmatrix} 4.7382 \\ -1.5080 \\ -1.6597 \\ 0.9815 \\ 1.0000 \\ 0.3751 \end{bmatrix}$	N/A	N/A
$\Delta\mathbf{V}(t_1)$ [m/s]	$0.0083\,\mathbf{i} + 0.0491\,\mathbf{k}$	$0.0345\,\mathbf{j}$	$0.0126\,\mathbf{i}$
$\Delta\mathbf{V}(t_2)$ [m/s]	$0.4896\,\mathbf{j}$	$0.3714\,\mathbf{k}$	$0.1570\,\mathbf{k}$
$\Delta\mathbf{V}(t_3)$ [m/s]	$0.3530\,\mathbf{k}$	$0.4854\,\mathbf{j}$	$0.5530\,\mathbf{j}$
$\Delta\mathbf{V}(t_4)$ [m/s]	$-0.4984\,\mathbf{i} + 0.4730\,\mathbf{j}$	$-0.5097\,\mathbf{i} + 0.4387\,\mathbf{j}$	$-0.5540\,\mathbf{i} + 0.3617\,\mathbf{j}$
Sequence cost [m/s]	1.8714	1.8397	1.6384
Computational cost [s]	0.1924	4.3322	0.8447

As may be observed, the results cannot be reproduced exactly in quantitative terms, although they do match qualitatively. The difference between all solvers is associated with a possible difference in the definition of the unit system by Serra et al. with respect to the Earth-Moon model used in this work, which was not included in the original manuscript [35]. Still, in both cases, the reference sequence cost solution in the literature is within the 90% of that computed by our solvers. However, their performance is satisfactory, especially when considering that only iterations are required to complete the optimization – compared to a complete SDP optimization in the solver by Serra et al. Note that the computational time is only provided for future reference, as they cannot be compared –the hardware setup between the papers is different as well. Still, our direct solvers compares to the indirect method by Serra et al., and our indirect methodology outperforms that of Serra and co-authors by a speed-up factor of at least 2. The rendezvous non-dimensional error is in the order of 10^{-15} for both fuel-consumption proxies. It is interesting to note that the problem is very sensitive to the discretization grid: for the l_1-rendezvous, both Neustadt and the direct solver find the very same impulsive anchor epochs; however, for the l_2-case, the direct solver is not able to correctly concentrate all maneuvers, leading to a sequence with an additional impulse to the optimal one. Still, in this case, they accumulate in the time vecinities of the control plan computed via Neustadt. This a natural result of the chaotic dynamics of the CR3BP.

Table 2 Trajectory optimization results for Scenario I, $p = 2$.

	Neustadt Solver	Direct Solver	Serra et al. [35]
N	100	100	1000
ρ	$N^{-3/2}$	N	N/A
N^*	2	3	2
$\boldsymbol{\lambda}$	$\begin{bmatrix} 3.000 \\ -1.098 \\ -0.918 \\ 0.536 \\ 0.681 \\ 0.329 \end{bmatrix}$	N/A	N/A
$\Delta\mathbf{V}(t_1)$ [m/s]	$[0.0127, 0.4805, 0.3686]$	$[0.0052, 0.2993, 0.2299]$	$[-0.0181, 0.5173, 0.1541]$
$\Delta\mathbf{V}(t_2)$ [m/s]	$[-0.4860, 0.5023, 0.0197]$	$[0.0018, 0.1821, 0.1393]$	$[-0.5677, 0.4595, 0.0165]$
$\Delta\mathbf{V}(t_3)$ [m/s]	N/A	$[-0.4883, 0.4967, 0.0154]$	N/A
Sequence cost [m/s]	1.3050	1.3050	1.2251
Computational cost [s]	0.6309	1.8520	1.3731

Both the optimal state-control trajectories as well as the primer vector norm evolution –for the two fuel-consumption proxies considered– are depicted in Figs. 2, 3 and 4, respectively.

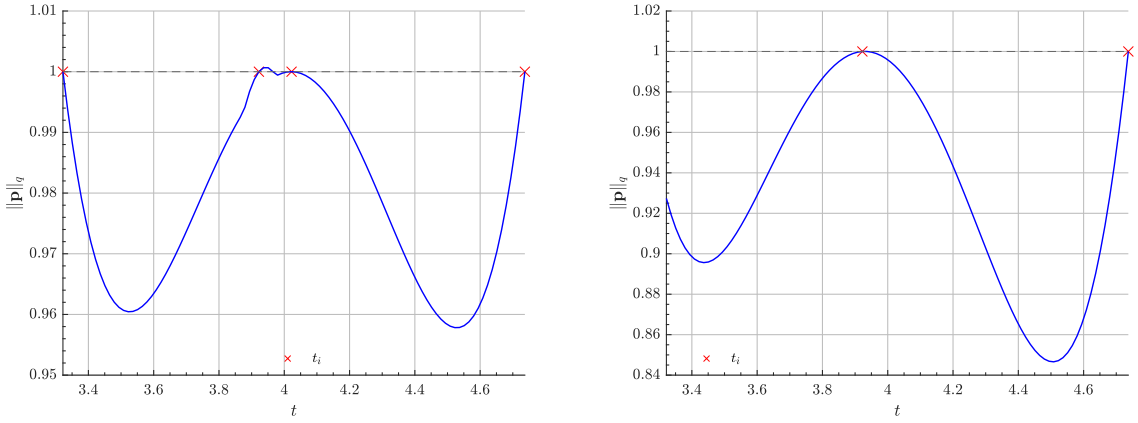

(a) Primer vector norm solution for $p = 1$. **(b) Primer vector norm solution for $p = 2$.**

Fig. 2 Primer vector norm history for Scenario I with l_p-cost.

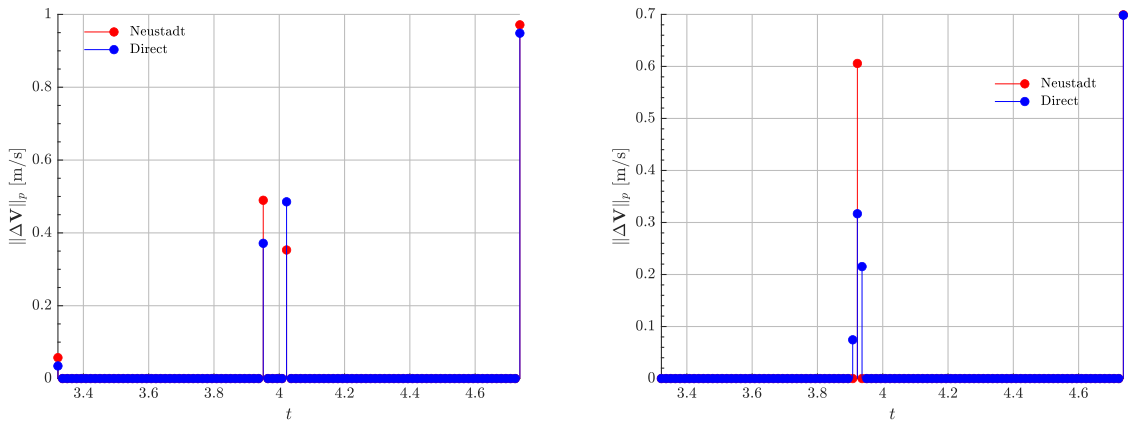

(a) Maneuver plan for $p = 1$. **(b) Maneuver plan for $p = 2$.**

Fig. 3 Optimal maneuver plan for Scenario I with l_p-cost.

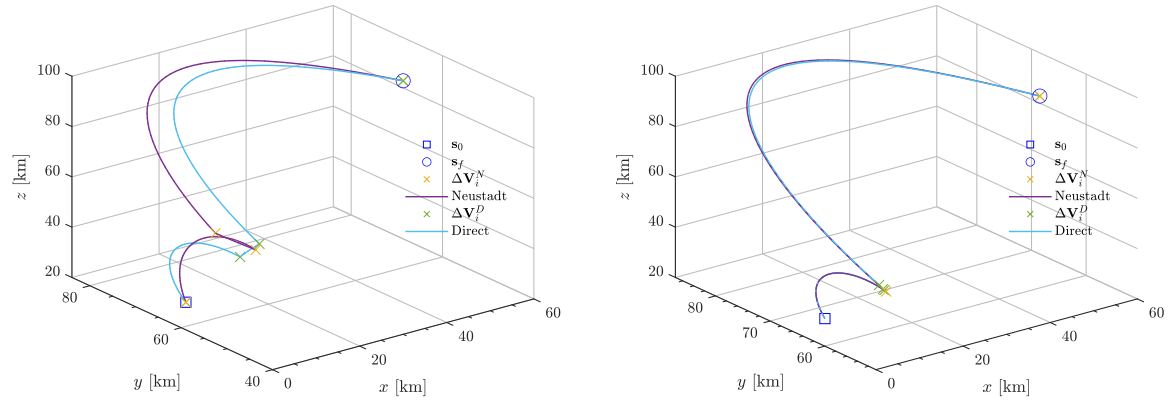

(a) Trajectory evolution for $p = 1$. **(b) Trajectory evolution for $p = 2$.**

Fig. 4 Optimal trajectory in co-orbital synodic position space for Scenario I with l_p-cost.

7.3 Fuel-optimal rendezvous between halo orbits

A second, more realistic mission example is provided by a halo-to-halo orbit transfer with timing constraints in the Earth-Moon system. Consider a chaser and a target spacecraft in an L_2 northern and southern halo orbit, respectively. The initial (nondimensional) conditions of the latter and the co-orbital state are given by

$$[\mathbf{r}_t, \dot{\mathbf{r}}_t]\,(t_0) = \begin{bmatrix} 0.824024728136525 & 0 & -0.054501847320725 & 0 & 0.164671964079122 & 0 \end{bmatrix}^\mathsf{T},$$
$$\mathbf{s}(t_0) = \begin{bmatrix} -0.000385289210804 & 0 & 0.097783417040814 & 0 & -0.012103983186502 & 0 \end{bmatrix}^\mathsf{T}.$$

These correspond to an initial miss-distance of 37594 km, thus providing a very challenging orbital transfer problem. The l_2 fuel-optimal rendezvous is to be achieved in a chaser's orbital period, approximately $t_f - t_0 = 2.7549$ nondimensional time units.

The transfer is to be performed by the proposed MPC scheme, with sampling time $T_s = 0.028$ –approximately, 2 hours 53 minutes–, as well as prediction and control horizons of $N = 100$ steps. Even though the target orbit is not close to that of the chaser, the RLLM dynamics is used to model the co-orbital motion between the two vehicles. In this sense, the dynamical mismatch between the RLLM and the true nonlinear plant is understood as dynamical noise, proving the MPC design under general uncertainty.

The sub-optimal MPC transfer between the two halos is computed through the primal ADMM solver, to provide a computational worst-case scenario. Once the transfer is solved, both the control solution, the resulting trajectory and the computational cost of each optimization across the mission timeline are shown in Figs. 5 to 6.

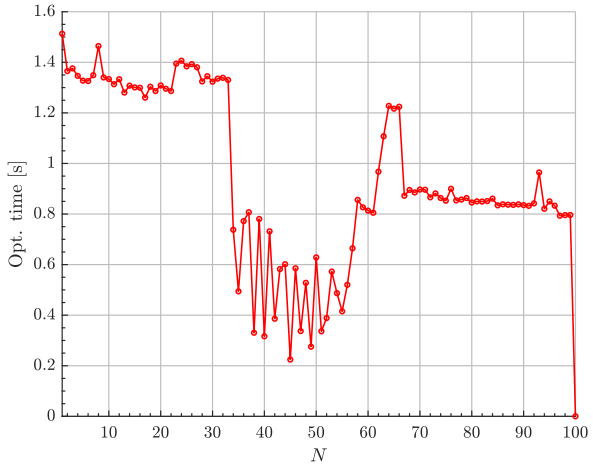

Fig. 5 Computational cost of each optimization under the MPC scheme for Scenario II.

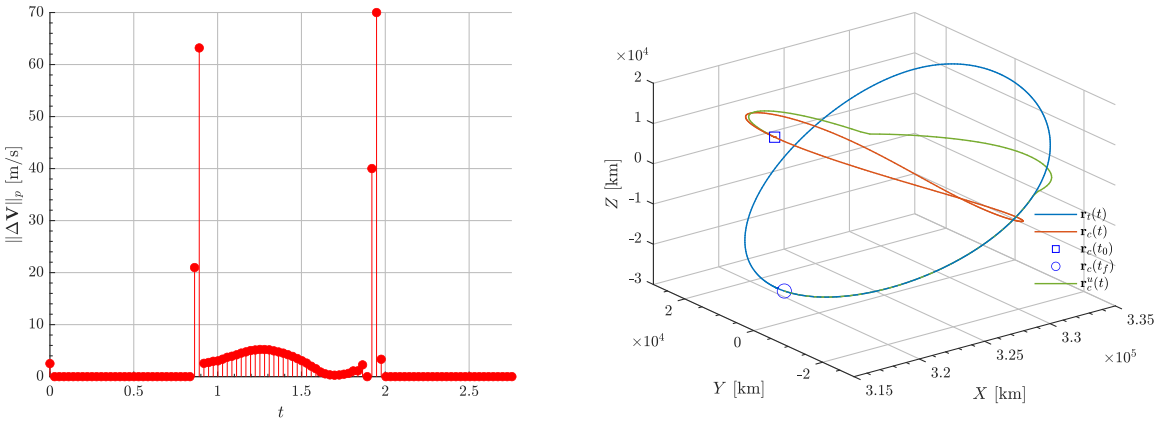

(a) MPC maneuver plan for $p = 2$. **(b) MPC synodic position trajectory for $p = 2$.**

Fig. 6 MPC control-state trajectory pair for Scenario II under l_2-cost.

As may be observed, each optimization remains under the 2-second benchmark, which outlines the applicability of this MPC design for real-time guidance, even under higher bandwidth of the designed control loop. Moreover, despite the initial miss-distance, the rendezvous is accomplished with an error of 2.34×10^{-6}; in dimensional units, this corresponds to 439.92 m and 2 mm/s of relative position and velocity, respetively. The total cost of the sequence is 304.5375 m/s.

To assess the optimality of the solution, these results are compared against the mission design obtained using a Chebyshev pseudospectral solver [71], which features the full nonlinear dynamics of the CR3BP, Eqs. (1). The comparison is achieved for the worst-case scenario, for $N = 100$ time nodes. Fig. 7 provides the resulting optimal, control-state trajectory. The corresponding performance comparison between methodologies is found next in Table 3.

To assess the CPU use of the MPC scheme, the computational cost of all N optimizations are considered together. Still, even under this complex metric, it is clear that the method clearly outperforms the PS solver in this sense, further considering the requirements of the latter in terms of numerical

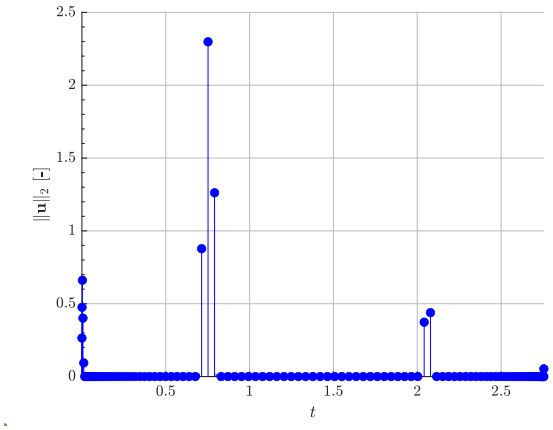

(a) Chebyshev PS maneuver plan for $p = 2$.

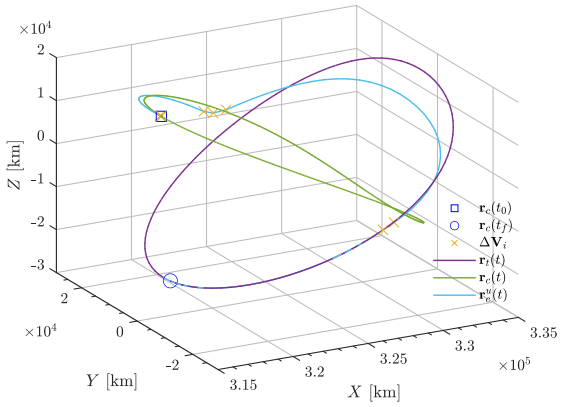

(b) PS synodic position trajectory for $p = 2$.

Fig. 7 PS control-state trajectory pair for Scenario II under l_2-cost.

Table 3 Comparison of trajectory optimization results for Scenario II, $p = 2$.

	MPC-Primal	**Chebyshev PS**
Sequence cost [m/s]	304.5375	211.2
Computational cost [s]	94.01	751.01

machinery –those of a NLP solver– against pure modular arithmetic operations within the ADMM algorithm. This advantages the latter for real-time guidance. The trade-off, of course, is suboptimality of the resulting MPC fuel consumption, which increases up to a 30%. Despite this discrepancy, note that both solving strategies cluster the maneuvers around the very nondimensional epochs, at $t = 0.75$ and close to $\ddot{=}2$.

The disparity between the two methods in terms of fuel consumptions may be explained by several factors. First, the chaotic behavior of the CR3BP –especially in the vecinities of dynamical bifurcations between orbits, as in this case– is excited by an ad-hoc selection of the prediction horizon N of the MPC scheme. Choosing an optimal prediction and control horizon to enhance the performance of the MPC close-loop remains an open line of research. Second, the orbital transfer clearly operates outside of any linearized regime, making non-captured, nonlinear effects dominant when describing the co-orbital motion of the chaser. For example, exploitation of hyperbolic co-orbital manifolds between the target and departure halos is not possible under the RLLM model, while indeed available for the PS solver. This really goes against the nature of the MPC-primal solver and its fundamental optimality conditions (Bellman's principle).

To assess the impact of the latter, the same experiment is completed in this case using the RLM model. At each sampling epoch, a numerical STM is computed via integration of the RLM model with the latest available target's state information, thus providing the primal solver with more accurate variational information. The results for the transfer computed under this setting in comparison with those obtained previously are shown next in Table 4.

Table 4 Comparison of trajectory optimization results for Scenario II, $p = 2$.

	MPC-Primal (RLM)	**MPC-Primal (RLLM)**	**Chebyshev PS**
Sequence cost [m/s]	429.9452	304.5375	211.2
Computational cost [s]	78.85	94.01	751.01

As may be observed, the use of another dynamical model exploits a different transfer solution. The higher-fidelity properties of the RLM model lead to a speed-up in convergence for each iteration of the MPC design; while leading in this case to greater fuel-consumption. Again, and even more relevantly, an appropriate selection of the control and prediction horizons N determines the performance of the method: for example, the ability to exploit these co-orbital invariant manifolds and natural co-orbital trajectories. The necessary sensitivity analyses of the complete MPC integral design to guide this selection is beyond the scope of this exploratory work, and provides a promising, open line of research.

8 Conclusions

The aim of this investigation is the introduction of a novel, inexpensive and conceptually simple numerical solver for general nonlinear fuel-optimal rendezvous problems.

In particular, candidate $\mathcal{L}_{1,p}$-norm fuel-optimal control sequences are generated through a recently introduced optimal control solver. The algorithm emerges as an Alternating Direction Method of Multipliers implementation of classical Primer Vector Theory, enabling closed-form algorithmic solutions to both constrained and unconstrained linear rendezvous problems. Under this setting, the solution process is powered by simple iterations of proximal minimizations, without the need of any advanced numerical machinery or dedicated optimization software but any efficient linear system solver. All in all, the combination of these two techniques allows to render general NLP fuel-optimal problems solvable by Linear Programming techniques. By means of classical, time-shrinking Model Predictive Control, the methodology can be further extended for nonlinear systems: the cost-efficient capabilities of the algorithm can be exploited as the inner optimization engine of an outer MPC loop. Overall, the proposed control architecture features a real-time oriented, integral guidance and control close-loop design.

Given its prominence and relevance for the near-future of the Space Industry, the performance of the solvers is demonstrated in the design of several benchmark rendezvous and orbital transfers in the Earth-Moon CR3BP. These provide objective mission scenarios in which to compare the performance of the proposed close-loop guidance-control design against previous literature efforts in the design of numerical fuel-optimal solving algorithms. Comparing its performance and capabilities with these state-of-the-art optimization techniques, the proposed solver stands as a solid candidate for real-time, embedded guidance applications, matching them in performance and accuracy without the need of dedicated or advanced numerical machinery.

Acknowledgments

S.C.d.V., H.U. and P.S.-L. wish to acknowledge the Spanish State Research Agency for their support through the Research Grant PID2024-161963OB-C21 funded by MICIU/ AEI / 10.13039/501100011033 / FEDER, UE.

Declaration of Use of Artificial Intelligence

Artificial intelligence was not used in the work presented.

References

[1] NASA. Nasa artemis. https://www.nasa.gov/artemis/, 2023. Accessed: 2023-09-28.

[2] S. Cuevas del Valle, H. Urrutxua, P. Solano-López, R. Gutierrez-Ramon, and A. K. Sugihara. Relative dynamics and modern control strategies for rendezvous in libration point orbits. *Aerospace*, 9(12), 2022. ISSN: 2226-4310. doi: 10.3390/aerospace9120798.

[3] W. Koon, M. Lo, J. Marsden, and S. Ross. *Dynamical Systems, the Three-Body Problem and Space Mission Design*. Marsden Books, Wellington, New Zealand, 2008.

[4] T.N. Edelbaum. How many impulses? *Astronautics and Aeronautics*, pages 64–69, 1967.

[5] D.F. Lawden. Optimal trajectories for space navigation. *Butterworths*, 1963.

[6] L.W Neustadt. Optimization, a moment problem, and nonlinear programming. *Journal of The Society for Industrial and Applied Mathematics, Series A: Control*, 2:33–53, 1964.

[7] R.G. Stern and J.E. Potter. *Optimization of Midcourse Velocity Corrections*, pages 70–83. 1966.

[8] J.E. Prussing. *Optimal multi-impulse orbital rendezvous*. PhD thesis, Massachusetts Institute of Technology, 1967.

[9] P. M. Lion and M. Handelsman. Primer vector on fixed-time impulsive trajectories. *AIAA Journal*, 6(1):127–132, 1968. doi: 10.2514/3.4452.

[10] D. Jezewski. Primer vector theory applied to the linear relative-motion equations. *Optimal Control Applications and Methods*, 1(4):387–401, 1980. doi: https://doi.org/10.1002/oca.4660010408.

[11] T. E. Carter. State transition matrices for terminal rendezvous studies: Brief survey and new example. *Journal of Guidance, Control, and Dynamics*, 21(1):148–155, 1998. doi: 10.2514/2.4211.

[12] E. Taheri and J.L. Junkins. How many impulses redux. *The Journal of the Astronautical Sciences*, 67:257–334, 2020.

[13] K. Saloglu, E. Taheri, and D. Landau. Existence of infinitely many optimal iso-impulse trajectories in two-body dynamics. *Journal of Guidance, Control, and Dynamics*, 07 2023. doi: 10.2514/1.G007409.

[14] G. Bucchioni, G. Gemignani, F. Lombardi, A. Bellome, J. Leitão, S. Lizy-Destrez, and M Innocenti. Optimal time-fixed impulsive non-keplerian orbit to orbit transfer algorithm based on primer vector theory. page 107307, 05 2023. doi: 10.1016/j.cnsns.2023.107307.

[15] R. Russell. Primer vector theory applied to global low-thrust trade studies. *Journal of Guidance Control and Dynamics*, 30:460–472, 03 2007. doi: 10.2514/1.22984.

[16] K. Bokelmann and R. Russell. Optimization of impulsive europa capture trajectories using primer vector theory. *The Journal of the Astronautical Sciences*, 67, 05 2019. doi: 10.1007/s40295-018-00146-z.

[17] C. Zhang, F. Topputo, F. Bernelli-Zazzera, and Y-S. Zhao. Low-thrust minimum-fuel optimization in the circular restricted three-body problem. *Journal of Guidance, Control, and Dynamics*, 38:1–9, 03 2015. doi: 10.2514/1.G001080.

[18] I.M. Ross. Space trajectory optimization and l1-optimal control problems. In P. Gurfil, editor, *Modern Astrodynamics*, volume 1 of *Elsevier Astrodynamics Series*, pages 155–VIII. Butterworth-Heinemann, 2006. doi: https://doi.org/10.1016/S1874-9305(07)80008-2.

[19] R. Barr and E. Gilbert. Some efficient algorithms for a class of abstract optimization problems arising in optimal control. *IEEE Transactions on Automatic Control*, 14(6):640–652, 1969. doi: 10.1109/TAC.1969.1099299.

[20] E. Gilbert and G. Harasty. A class of fixed-time fuel-optimal impulsive control problems and an efficient algorithm for their solution. *IEEE Transactions on Automatic Control*, 16(1):1–11, 1971. doi: 10.1109/TAC.1971.1099656.

[21] X. Liu, P. Lu, and B. Pan. Survey of convex optimization for aerospace applications. *Astrodynamics*, 1, 02 2017. doi: 10.1007/s42064-017-0003-8.

[22] D. Malyuta, Y. Yu, P. Elango, and B. Açïkmeçe. Advances in trajectory optimization for space vehicle control. *Annual Reviews in Control*, 52:282–315, 2021. ISSN: 1367-5788. doi: https://doi.org/10.1016/j.arcontrol.2021.04.013.

[23] L. Breger and J. How. J2-modified gve-based mpc for formation flying spacecraft. 08 2012. doi: 10.2514/6.2005-5833.

[24] E. N. Hartley. A tutorial on model predictive control for spacecraft rendezvous. In *2015 European Control Conference (ECC)*, pages 1355–1361, 2015. doi: 10.1109/ECC.2015.7330727.

[25] R. Vazquez, F. Gavilan, and E.F. Camacho. Model predictive control for spacecraft rendezvous in elliptical orbits with on/off thrusters. *IFAC-PapersOnLine*, 48(9):251–256, 2015. ISSN: 2405-8963. 1st IFAC Workshop on Advanced Control and Navigation for Autonomous Aerospace Vehicles ACNAAV'15. doi: https://doi.org/10.1016/j.ifacol.2015.08.092.

[26] F. Gavilan, R. Vazquez, and E. F. Camacho. Chance-constrained model predictive control for spacecraft rendezvous with disturbance estimation. *Control Engineering Practice*, 20(2):111–122, 2012. ISSN: 0967-0661. doi: https://doi.org/10.1016/j.conengprac.2011.09.006.

[27] J. Sánchez, F. Gavilán, and R. Vázquez. Chance-constrained model predictive control for near rectilinear halo orbit spacecraft rendezvous. *Aerospace Science and Technology*, 100:105827, 03 2020. doi: 10.1016/j.ast.2020.105827.

[28] A. Capannolo, G. Zanotti, M. Lavagna, and G. Cataldo. Model predictive control for formation reconfiguration exploiting quasi-periodic tori in the cislunar environment. *Nonlinear Dynamics*, 111, 01 2023. doi: 10.1007/s11071-022-08214-8.

[29] M. Mammarella, E. Capello, and G. Guglieri. Robust model predictive control for automated rendezvous maneuvers in near-earth and moon proximity. 09 2018. doi: 10.2514/6.2018-5343.

[30] M. Pagone, M. Boggio, C. Novara, and S. Vidano. A pontryagin-based nmpc approach for autonomous rendez-vous proximity operations. In *2021 IEEE Aerospace Conference (50100)*, pages 1–9, 2021. doi: 10.1109/AERO50100.2021.9438226.

[31] Michele Pagone, Giordana Bucchioni, Francesco Alfino, and Carlo Novara. A minimum-propellant pontryagin-based nonlinear mpc for spacecraft rendezvous in lunar orbit: the extended version, 2023.

[32] D. Arzelier, M. Kara-Zaitri, C. Louembet, and A. Delibasi. Using polynomial optimization to solve the fuel-optimal linear impulsive rendezvous problem. *Journal of Guidance, Control, and Dynamics*, 34, 09 2011. doi: 10.2514/1.52227.

[33] D. Arzelier, C. Louembet, A. Rondepierre, and M. Kara-Zaitri. A new mixed iterative algorithm to solve the fuel-optimal linear impulsive rendezvous problem. *Journal of Optimization Theory and Applications*, 159, 10 2013. doi: 10.1007/s10957-013-0282-z.

[34] D. Arzelier, F. Bréhard, N. Deak, M. Joldes, C. Louembet, A. Rondepierre, and R. Serra. Linearized impulsive fixed-time fuel-optimal space rendezvous: A new numerical approach. *IFAC-PapersOnLine*, 49:373–378, 2016.

[35] R. Serra, D. Arzelier, F. Bréhard, and M. Joldes. Fuel-optimal impulsive fixed-time trajectories in the linearized circular restricted 3-body-problem. 10 2018.

[36] C. Louembet. *Contributions au guidage pour le rendez-vous spatial par résolution du problème de commande optimale impulsionnelle*. PhD thesis, Université Toulouse, 2017.

[37] M. Claeys, D. Arzelier, D. Henrion, and J.-B. Lasserre. Measures and lmi for impulsive optimal control with applications to space rendezvous problems. *Proceedings of the American Control Conference*, 10 2011. doi: 10.1109/ACC.2012.6315549.

[38] M. Claeys, D. Arzelier, D. Henrion, and J.-B. Lasserre. Moment lmi approach to ltv impulsive control. *Proceedings of the IEEE Conference on Decision and Control*, 03 2013. doi: 10.1109/CDC.2013.6760805.

[39] A. W. Koenig and S. D'Amico. Fast algorithm for fuel-optimal impulsive control of linear systems with time-varying cost. *IEEE Transactions on Automatic Control*, 66(9):4029–4042, 2021. doi: 10.1109/TAC.2020.3027804.

[40] Ethan Foss and Simone D'Amico. Efficient input-constrained impulsive optimal control of linear systems with application to spacecraft relative motion. *arXiv preprint arXiv:2510.03423*, 2025.

[41] S. Le Cleac'h and Z. Manchester. Fast solution of optimal control problems with l1 cost. In *Proceedings of AAS/AIAA Astrodynamics Specialist Conference*, 2019.

[42] K. Tracy and Z. Manchester. Model-predictive attitude control for flexible spacecraft during thruster firings. In *Proceedings of the AAS-AIAA Astrodynamics Specialist Conference*, 2020.

[43] L. Persson. *Model Predictive Control for Cooperative Rendezvous of Autonomous Unmanned Vehicles*. PhD thesis, KTH Royal Institute of Technology, 2021.

[44] S. Cuevas del Valle, P. Solano-López, and H. Urrutxua. A dual-based linear programming formulation of optimal control: Fuel-optimal rendezvous guidance and boresight pointing applications. July 2023. doi: 10.13009/EUCASS2023-057.

[45] S. Cuevas del Valle, H. Urrutxua, and P. Solano-López. Proximal operators and duality for linear fuel-optimal rendezvous. *Currently under review*, 2025.

[46] R. J. Luquette. *Nonlinear control design techniques for precision formation flying at Lagrange points*. PhD thesis, University of Maryland, 2006.

[47] S. Cuevas del Valle, H. Urrutxua, and P. Solano-López. Optimal floquet stationkeeping under the relative dynamics of the three-body problem. *Aerospace*, 10(5), 2023. ISSN: 2226-4310. doi: 10.3390/aerospace10050393.

[48] David L. Richardson. A note on lagrangian formulations for motion about the collinear points. *Celestial Mechanics*, 22:231–236, 1980. doi: 10.1007/BF01229509.

[49] S. Cuevas del Valle, V. Ribera, and H. Urrutxua. Cost-efficient reachable set determination with applications in attitude control. *In preparation.*, 2025.

[50] I.M. Ross. *A Primer on Pontryagin's Principle in Optimal Control*. 2015. ISBN: 978-0984357116.

[51] M. Leomanni, G. Bianchini, A. Garulli, A. Giannitrapani, and R. Quartullo. Sum-of-norms model predictive control for spacecraft maneuvering. *IEEE Control Systems Letters*, 3(3):649–654, 2019. doi: 10.1109/LCSYS.2019.2915152.

[52] J.E. Prussing. *Primer Vector Theory and Applications*, pages 16–36. 2010.

[53] J.E. Prussing and R.S. Clifton. Optimal multiple-impulse satellite evasive maneuvers. *Journal of Guidance, Control, and Dynamics*, 17(3):599–606, 1994. doi: 10.2514/3.21239.

[54] T. E. Carter. Necessary and sufficient conditions for optimal impulsive rendezvous with linear equations of motion. *Dynamics and Control*, 10(1):219–227, 2000. doi: 10.1023/A:1008376427023.

[55] L. W. Neustadt. A general theory of minimum-fuel space trajectories. *Journal of the Society for Industrial and Applied Mathematics Series A Control*, 3(2):317–356, 1965. doi: 10.1137/0303023.

[56] M. Kara-Zaitri, D. Arzelier, A. Delibasi, and C. Louembet. Polynomial optimization for the solution of fuel-optimal impulsive rendezvous using primer vector theory. pages 352–357, 12 2010. doi: 10.1109/CDC.2010.5717372.

[57] S. Boyd, E. Parikh, N.Chu, B. Peleato, and J. Eckstein. *Distributed Optimization and Statistical Learning via the Alternating Direction Method of Multipliers*. Standford University, 2010.

[58] D. Gabay and B. Mercier. A dual algorithm for the solution of nonlinear variational problems via finite element approximation. *Computers & Mathematics With Applications*, 2:17–40, 1976.

[59] R. Glowinski and A. Marroco. Sur l'approximation, par éléments finis d'ordre un, et la résolution, par pénalisation-dualité d'une classe de problèmes de Dirichlet non linéaires. *Revue française d'automatique, informatique, recherche opérationnelle. Analyse numérique*, 9(R2):41–76, 1975.

[60] J. Eckstein and D.P. Bertsekas. On the douglas-rachford splitting method and the proximal point algorithm for maximal monotone operators. *Mathematical Programming*, pages 293–318, 04 1992. doi: 10.1007/BF01581204.

[61] N Parikh and S. Boyd. *Proximal Algorithms*. Standford University, 2013.

[62] G. Banjac, P. Goulart, B. Stellato, and S. Boyd. Infeasibility detection in the alternating direction method of multipliers for convex optimization. *Journal of Optimization Theory and Applications*, 183(2):490–519, 2019. doi: 10.1007/s10957-019-01575-y.

[63] E.F. Camacho and C. Bordons. *Model Predictive Control*. Springer, 1998. ISBN: 978-0-85729-398-5.

[64] M. Schwenzer, M. Ay, T. Bergs, and D. Abel. Review on model predictive control: an engineering perspective. *The International Journal of Advanced Manufacturing Technology*, 117:1327–1349, 2021.

[65] A. Richards and J. How. Performance evaluation of rendezvous using model predictive control. *AIAA Guidance, Navigation, and Control Conference and Exhibit*, 11 2003. doi: 10.2514/6.2003-5507.

[66] A. Richards and J. How. Analytical performance prediction for robust constrained model predictive control. *International Journal of Control*, 79, 08 2006. doi: 10.1080/00207170600699740.

[67] I. Ross, Pooya Sekhavat, Andrew Fleming, and Qi Gong. Optimal feedback control: Foundations, examples, and experimental results for a new approach. *Journal of Guidance Control and Dynamics - Journal of Guidance, Control, and Dynamics*, 31:307–321, 03 2008. doi: 10.2514/1.29532.

[68] S. Gros, M. Zanon, R. Quirynen, A. Bemporad, and M. Diehl. From linear to nonlinear mpc: bridging the gap via the real-time iteration. *International Journal of Control*, 93:1–19, 09 2016. doi: 10.1080/00207179.2016.1222553.

[69] Mathworks. Matlab 2021b. `https://es.mathworks.com/products/new_products/release2021b.html`. Accessed: 2023-08-31.

[70] B. Stellato, G. Banjac, P. Goulart, A. Bemporad, and S. Boyd. OSQP: an operator splitting solver for quadratic programs. *Mathematical Programming Computation*, 12(4):637–672, 2020. doi: 10.1007/s12532-020-00179-2.

[71] Qi Gong, I. Michael Ross, and Fariba Fahroo. A chebyshev pseudospectral method for nonlinear constrained optimal control problems. In *Proceedings of the 48h IEEE Conference on Decision and Control (CDC) held jointly with 2009 28th Chinese Control Conference*, pages 5057–5062, 2009. doi: 10.1109/CDC.2009.5400509.